Impact of phase and amplitude variations in the performance of an InP optical phased array

M. Gagino,[1] K.A. Williams[1], M. Smit[1], E.A.J.M. Bente[1], V. Dolores-Calzadilla[1,2]

[1] Technical University Eindhoven, Dept. of Electrical Engineering, Groene Loper 19, 5612 AP Eindhoven, The Netherlands

[2] Photonic Integration Technology Center, Groene Loper 19, 5612 AP Eindhoven, the Netherlands

We present a simulation study of a non-ideal optical phased array (OPA) with 8 channels operating at 1550nm, which has amplitude and phase control. We consider an OPA which suffers from etching lag effect, as well as phase and amplitude variations. The ideal OPA response produces a far field with 7 resolvable spots and -19.6dB diffraction sidelobes suppression ratio (SSR). When considering a random phase variation of ±20% of π rad, the number of resolvable spots remains unchanged and the SSR is <-11dB. Therefore, we conclude that the OPA performance is not significantly degraded for such strong phase variations. Furthermore, we show that typical voltage dependent electro-absorption losses of phase shifters can be tolerated, thereby simplifying architectures for gain control.

Introduction

Optical phased arrays (OPAs) have gained attention in research thanks to their ability to perform beam shaping and steering on a photonic integrated circuit (PIC) with no moving parts, thus giving potential advantages such as high steering speed and scalability, which are of interest in applications like LiDAR and free space optical communication [1, 2, 3]. Moreover, InP platforms for PICs makes it possible to integrate semiconductor optical amplifiers (SOAs), electro-optic phase modulators (EOPMs) and tunable lasers on the same chip to emit high-power steerable optical beams.

In order to study the far field properties of an OPA beam, we designed an optical phased array with phase and amplitude control in all arms, and we simulated the behavior of its beam across its field of view (FoV, i.e., angular range before aliasing occurs). The shape of the emitter waveguides was considered as a simulation parameter to study the impact of the so-called lag effect [4], which determines an under-etching of waveguide in dense arrays.

The channels of an OPA can also be affected by phase errors that deteriorate the quality of the optical beam. These uncertainties may be attributed to fabrication tolerance of waveguide widths, layerstack thickness and roughness [5], as well as the accuracy of the OPA calibration method. Additionally, amplitude variations may occur due to electro-absorption of EOPMs [6, 8]. To determine the effect on the OPA beam properties of such fluctuations, we applied randomly distributed values of phase and amplitude across the OPA channels, and we carried out far field simulations. We based the simulations on an 8-channel OPA device which was designed and manufactured in a InP generic platform.

Design of chip

We designed a ±20° FoV OPA with 8 channels capable of phase and amplitude control (Figure 1a). The power from the input waveguide is distributed in several channels through a star coupler with -6dB non-uniformity (i.e., the power ratio between outer and inner arms). The OPA emits into free space through an array of edge-emitting parallel

waveguides whose width and pitch are 1.2µm and 2.2µm, respectively; the waveguides are deep-etched to minimize optical crosstalk while reducing the pitch to ensure a wide FoV.

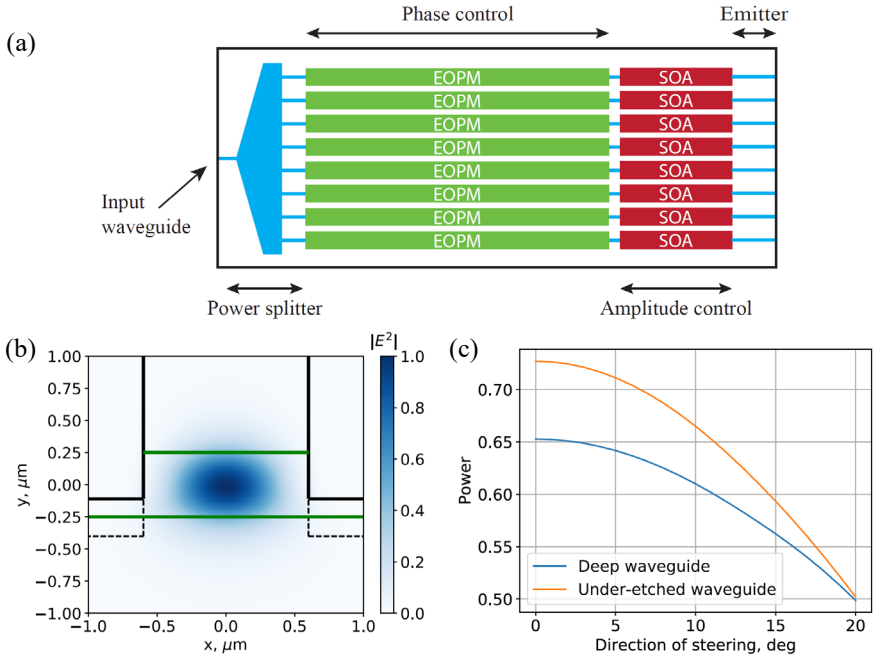

Figure 1: (a) Schematic of the designed OPA. (b) Fundamental TE mode of an under-etched 1.2µm-wide waveguide. The waveguide profile is drawn in black, and its core is highlighted in green; the dashed lines show the profile of an ideal fully etched deep waveguide. (c) Main beam power ratio across 180° steering range for fully-etched and under-etched emitter waveguides.

Simulations

In order to study the emission profiles of the previously described 8-channel OPA, we simulated the emitter waveguide fundamental TE modes in Lumerical MODE (FDE). We considered the case of a 1.2µm wide deep-etched waveguide with InP generic platform layerstack and ideal deep etch level [7], and we compared it with a 14% under-etched waveguide (Figure 1b). From the single waveguide modes, we obtained the 2D near field, which was then propagated into the far field using Lumerical FDTD. The near field profile generated by under-etched waveguides was modified with phase and amplitude variations in the OPA arms. For this study, we generated random phase and amplitude values within the ±π/4 rad and ±50% ranges. For each simulation, the values of phase and amplitude were randomly drawn 200 times with uniform distribution.

Results

The effect of the emitter waveguides under-etching on the OPA performance is quantified by the percentage of power in the main beam at different steering angles: it is calculated as the intensity integral within the first two minima of the main beam divided by the total intensity integral (in the ±90° angular range), since the emitter shape has an impact in the radiation pattern envelope of the array. The simulation results presented in Figure 1c show that a 14% under-etch is beneficial to the power of the OPA beam for all angles in the steering range. In fact, the fundamental mode of an under-etched waveguide is 5% wider at the center of the core than the mode of a fully etched waveguide whose full-width at half-maximum (FWHM) is 0.624µm. This results in a 5% narrower Gaussian far field envelope which determines a higher suppression of the grating lobes, and an increased

power level in the main beam, which varies in the 50%-73% range across the steering range. However, the narrower Gaussian envelope causes a more abrupt variation of the beam peak intensity when it is steered: 23% variations across the steering range in the under-etch case and 15% in the ideal case. The angular resolution (FWHM), image resolution (FoV/FWHM), and the diffraction sidelobes suppression ratio (SSR) are independent from the shape of the emitter modes. For the OPA design we presented here, the simulated FWHM is 5.1°, the image resolution is 7, and the SSR is -19.6dB.

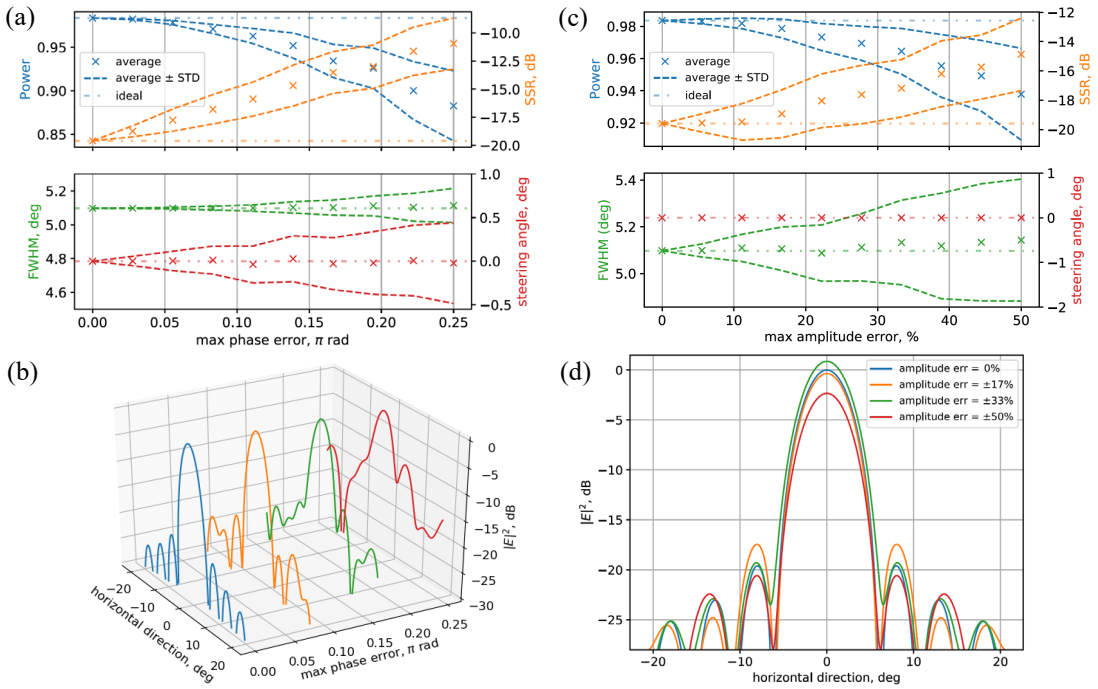

Figure 2: (a) Ratio of power in the main beam, SSR, angular resolution and steering angle at different phase error conditions. (b) Far field profiles with increasing phase error. (c, d) Simulation results for amplitude fluctuations.

We simulated the effects of phase and amplitude variations at a 0° fixed steering angle. The results presented in Figure 2a-b show the deterioration of far field beam properties with an increasing phase uncertainty in the OPA channels. In particular, the power ratio in the main beam with respect to the total power in the field of view drops from 98.3% in the ideal case to 88.2%±4.1% when the maximum phase error is in the ±π/4 rad range. The phase uncertainty in each arm contributes to de-focusing the beam, thus inducing an increase of the background level and the loss of power from the main beam. Under this condition, the simulated SSR of the under-etched OPA emitter is increased to -10.9dB ±2.2dB. Since each arm's reference phase was set to 0 rad, the average direction of steering is 0°. However, among the 200 simulated cases, the probability of the beam steering direction deviating by 0.4° is non-negligible at ±π/4 rad phase error, as shown in Figure 2a. Similarly, the angular resolution remains unchanged with 0.1° deviations. For the 8-channel OPA we described in this work, we can assume reasonable deviations from ideality when the power is reduced by <10%, the SSR is <-10dB and the image resolution is unchanged. Such condition occurs at ±20%π rad phase error: 8% power decrease, SSR <-11dB, 7 resolvable spots. Similar results are expected at any other steering angle.
When amplitude in the arms of the OPA fluctuates in the ±50% range, the power in the main beam and the SSR can deteriorate to 93.8%±2.8% and -14.9dB±2.5dB respectively,

as shown in Figure 2c-d. In this case the ideal beam shape is disturbed due to a reduced phase contribution from the arms whose amplitude is suppressed relatively to the amplified channels. The steering direction is independent from amplitude uncertainties, while the angular resolution is constant on average, with 0.3° deviations (Figure 2c). The negative fluctuations of FWHM with respect to the average value are due to the method employed to calculate it, which relies on the detection of the main beam minima: as both phase and amplitude errors increase, the background level raises as shown in the SSR plots of Figure 2c, and so do the beam minima. Consequently, the half-maximum position is shifted upwards, where the beam is narrower. Finally, a practical case can be considered when the amplitude in the OPA arms fluctuate in the ±2.25% range, which corresponds to the electro-absorption variations of an EOPM driven at voltages in the 0-10V range at 1550nm [8], the effects on the far field properties are negligible: the beam power, SSR, and FWHM are deviating from the ideal values by 0.5%, 0.3dB, and 0.01° respectively.

Conclusions

We presented the results of near and far field simulations of a 40° FoV OPA with phase and amplitude control and we showed that waveguides under-etching causes an 8% increase in the main beam power at 0° steering compared to the case with ideal deep-etched waveguide profile.

We demonstrated that phase fluctuations as high as $\pm 20\% \, \pi \, rad$ can cause a lowering of the main beam power by 8%, while the SSR is <-11dB and the number of resolvable spots is unchanged. It is thus possible to relax the constraints of phase accuracy during calibration procedures. Moreover, amplitude fluctuations in the ±2.25% range, as expected from electro-absorption of the phase modulators, produce a negligible effect on the beam properties. Therefore, the amplitude control in the OPA arms can be simplified by driving the SOAs at a constant bias point. Consequently, it might be possible to lower the number of driving signals connecting several SOAs in parallel.

Acknowledgments

This work has received funding support from the European Union's Horizon 2020 program through the NewControl project under grant no. 826653.

References

[1] H. Abediasl and H. Hashemi, "Monolithic optical phased-array transceiver in a standard SOI CMOS process", Optics Express, vol. 23, no. 5, p. 6509, 2015.

[2] T. Kim et al., "A Single-Chip Optical Phased Array in a Wafer-Scale Silicon Photonics/CMOS 3D-Integration Platform", IEEE Journal of Solid-State Circuits, vol. 54, no. 11, pp. 3061-3074, 2019.

[3] M. Heck, "Highly integrated optical phased arrays: photonic integrated circuits for optical beam shaping and beam steering", Nanophotonics, vol. 6, no. 1, pp. 93-107, 2017.

[4] J. Bolk et al., "Deep UV Lithography Process in Generic InP Integration for Arrayed Waveguide Gratings", IEEE Photonics Technology Letters, vol. 30, no. 13, pp. 1222-1225, 2018.

[5] T. Goh, S. Suzuki and A. Sugita, "Estimation of waveguide phase error in silica-based waveguides", Journal of Lightwave Technology, vol. 15, no. 11, pp. 2107-2113, 1997.

[6] J. Vinchant, J. Cavailles, M. Erman, P. Jarry and M. Renaud, "InP/GaInAsP guided-wave phase modulators based on carrier-induced effects: theory and experiment", Journal of Lightwave Technology, vol. 10, no. 1, pp. 63-70, 1992.

[7] L. Augustin et al., "InP-Based Generic Foundry Platform for Photonic Integrated Circuits", IEEE Journal of Selected Topics in Quantum Electronics, vol. 24, no. 1, pp. 1-10, 2018.

[8] S. Andreou, "Integrated Stabilized laser systems for high resolution strain and position sensing", PhD defense thesis, 2020.